IET Generation, Transmission & Distribution

Research Article

IET Journals
The Institution of Engineering and Technology

Supplementary automatic generation control using controllable energy storage in electric vehicle battery swapping stations

ISSN 1751-8687
Received on 30th March 2015
Revised on 31st October 2015
Accepted on 2nd December 2015
doi: 10.1049/iet-gtd.2015.0167
www.ietdl.org

Pingping Xie[1], Yinhong Li[1] ✉, Lin Zhu[1,2], Dongyuan Shi[1], Xianzhong Duan[1]

[1]*State Key Laboratory of Advanced Electromagnetic Engineering and Technology, School of Electrical and Electronic Engineering, Huazhong University of Science and Technology, Wuhan, People's Republic of China*
[2]*Department of Electrical Engineering and Computer Science, University of Tennessee at Knoxville, Knoxville, TN, USA*
✉ *E-mail: liyinhong@hust.edu.cn*

Abstract: One of the significant impacts of the growing penetration of intermittent renewable energy sources is upon the frequency response of power system. Compared with the dispersive electric vehicle energy storage, electric vehicle battery swapping station (BSS), as an emerging form of storage, can provide a more reliable supplementary regulation service for frequency control. This study has proposed a new supplementary automatic generation control (AGC) strategy using controllable energy storage in BSSs, referred to as station-to-grid (S2G). A Monte–Carlo stochastic simulation method is utilised to estimate the equivalent controllable capacity (CC) of BSSs, and then the lumped S2G equivalent model subject to SOC limits and CC constrains is presented. A filter-based AGC coordinated strategy is used to allocate the regulation power between generators and BSSs. The proposed AGC strategy is validated in a two-area interconnected power system with significant load and wind power fluctuations. Comparison analysis demonstrates the availability of the proposed models and control methods.

1 Introduction

Balancing the generation and demand to maintain a rated system frequency is a critical problem in power system operation and control. Traditionally, the frequency control methods are mainly achieved by adjusting the spare capacity on generation side to follow the stochastic demand through the automatic generation control (AGC) technology. Recently, since the high penetration of wind power and other renewable generation not only causes active power fluctuation on the generation side, but also decreases the equivalent inertia of the entire system, the frequency stability problem receives more and more concerns [1–3]. The report of the National Energy Technology Laboratory indicates that the conventional frequency control methods are facing both technical and economic challenges due to the increasing power imbalance and insufficient spare capacity [4].

Integrating the controllable resources within distribution systems into the conventional AGC program provides a new method to solve the frequency control problem [5]. In recent years, electric vehicles (EVs) are fast developing mainly due to environmental and energy security concerns. As a new form of battery storage, large-scale integration of EVs will bring new applications for optimal operation of power systems [6–10]. One of the most promising applications is to offer frequency regulation service through vehicle-to-grid (V2G) technology. Published papers have addressed the benefits, models and control strategies for V2G frequency regulation [11–17]. However, due to the randomness of the EV mobility, the complexity and uncertainty of system frequency control seem to be increased if each dispersed plugged-in EV should be controlled.

Actually, the battery storage in EV battery swapping stations (BSSs) has great potential to be reliably used. There have been several studies focusing on the planning, operation, and application of BSSs. An optimisation model for locating and sizing BSSs in distribution systems is proposed in [18]. In this model, the load type, required network reinforcements, and reliability of the system are explicitly considered. However, the swapping demand requirement is ignored. In [19], the charging load forecasting model for a BSS is studied, considering the hourly number of EVs, charging start time, travel distance, and charging duration. Some optimal operation strategies for batteries charging schedule in a BSS are discussed in [20–23]. In these works, the BSSs are modelled to minimise the energy cost, taking into account the real-time electricity prices, the state of charge (SOC) of depleted batteries, and the arrival times of EVs. For the application of BSSs, a photovoltaic (PV)-based BSS model is proposed in [24, 25] where the BSS is regarded as an energy storage station to store surplus electricity from PV plants. A charging strategy for the operation of the PV-based BSS considering the availability of service and the self-consumption of PV energy is proposed in [26]. The battery-swapping service model is used to guarantee EVs to swap batteries quickly without excess waiting. However, the stochastic properties of the swapping service time, waiting time, and battery charging time are not considered in this model.

Using the energy storage in BSSs for frequency regulation is an emerging application of EV batteries storage. However, the power of BSS storage cannot be changed freely. Like the major generation within distribution systems as well as the context of conventional generation control, some constraints must be met in the modelling of BSS storage due to the actual operation limits. For example, the SOC of the batteries in BSSs are supposed to be kept within some range during regulation for considering the customer expectation on battery SOC as well as the reduction in battery aging, and the responsive power should be subject to the controllable power and energy capacity of BSS storage.

The main concerns of this paper are focused on the modelling and control strategy of BSS storage. The interaction between BSS storage and power grid is termed as station-to-grid (S2G). A Monte–Carlo stochastic simulation (MCSS) method is proposed to estimate controllable capacity (CC) of BSS storage, and then a lumped equivalent model of S2G subject to SOC limits and CC constrains is presented. A filter-based coordinated control strategy is used in the AGC model considering S2G, which regards all the BSSs in the control area as a virtual energy storage station. Only the fast-cyclic component of the control signal will be dispatched to

BSS storage by the filter-based coordinated control strategy. The proposed AGC strategies are verified in a two-area interconnected power system with relatively large random load and wind power fluctuations. The simulation results and economic analysis demonstrate that the proposed strategies are feasible, and the energy storage in BSSs is a good supplementary resource for power system frequency control.

2 Descriptions of S2G participating in the AGC program

2.1 Concept of S2G

BSSs energy storage is an emerging form of storage which consists of EV batteries swapping and the station batteries charging. In this paper, we call the application scenarios of battery energy storage in BSSs for giving benefits to power grid as the concept of S2G. The S2G power, that is, the power of all the BSSs, can be adjusted when it is needed by the grid. Unlike V2G and traditional battery storage, the application of S2G storage needs to consider the user swapping demand and the station batteries charging schedules. The storage capacity is not constant, but varies with the number of controllable batteries (CBs) in BSSs of the control area.

2.2 Coordinated dispatching method among BSSs for S2G participating in AGC

The batteries in BSSs can be divided into three parts, that is, swapping batteries (used for EV batteries swapping), charging batteries (charging the depleted batteries up to a certain SOC level) and CBs. While S2G takes part in AGC, only the CBs can respond to the control signals. The dispatching of control signals among BSSs can be achieved by the SOC synchronisation control method proposed in [27]. This method consists of the coordination between central control centre (CCC) and local control centres (LCCs) (upper layer) and that between LCC and CBs (lower layer). In the lower layer, the charging/discharging priorities of the CBs are determined according to their SOCs. The charging signal is dispatched to the CBs in ascending order of the SOCs, whereas the discharging signal is dispatched in descending order of the SOCs. By using this coordinated dispatching method, the SOCs of the CBs in a BSS can be synchronised. In the upper layer, the charging/discharging priorities of the BSSs are determined according to their average SOCs. The CCC receives the information on the average SOC in each LCC and dispatches the control signals to the LCCs in the same manner. Consequently, no matter how many BSSs take part in the AGC program, the SOCs of all the CBs in the control area are synchronised so that the BSSs can be designed as one large-capacity virtual storage station (VSS). The average SOC of CBs can be regarded as the SOC of the VSS, which we call it virtual SOC (VSOC) in this paper.

3 Proposed S2G model

3.1 Battery SOC constraint

The SOCs of the CBs may fluctuate with the AGC signals. However, the EV users would not like to accept a battery with relatively low SOC for swapping. They may want the battery SOC to be higher than some level for the next trip. In this paper, it is assumed to be 0.8. Meanwhile, the SOC should be lower than some level (it is assumed to be 0.9 in this paper) for considering that the lifetime of battery becomes decreased by charging/discharging with nearly 100% of SOC [17]. That is to say, the SOCs of the CBs should be kept between 0.8 and 0.9 in this paper during regulation. Economic incentives can be given to the users who accept this requirement.

3.2 State transitions of batteries

As described above, the batteries in BSSs can be divided into three states, that is, swapping state, charging state, and controllable state. The state transition from the controllable state to the swapping state which we call it control-out happens at the time when EV begins to receive swapping service. It is noted that the time may not be the EV arrival time because there might be queues in batteries swapping. After the depleted battery has been swapped, it becomes the charging state from the swapping state which we call it swapping-out. The depleted battery cannot yet respond to the AGC signals. It needs to be charged up to a certain level of SOC (it is assumed to be 0.85 in this paper) at first. Similarly, there might be queues in this process. After the battery has been charged up to the object SOC, it becomes the controllable state which we call it control-in to respond to the AGC signals. The states of batteries in BSSs change among the three states continuously. Each battery has the different time at control-out, swapping-out, and control-in. Thus, the number of CBs will fluctuate dynamically.

3.3 Calculation of CC by MCSS

In this paper, we propose a MCSS method for calculating the CC of BSSs storage by simulating the queues in vehicle batteries swapping and depleted batteries charging.

It is assumed that there are n BSSs in the control area, and each BSS can provide services for m EVs. Like the arrival of customers in a gas station or a bank which is depicted in the queueing theory [28], the arrival of EVs at a BSS follows a Poisson process. Assuming the initial time is t_0, then the arrival time $t_{\text{as}}^{i,k}$ for the kth EV in the ith BSS can be determined by (1), where $\tau_{\text{s}}^{i,j}$ is the arrival time interval of two adjacent vehicles which follows an exponential distribution (i.e. $\tau_{\text{s}}^{i,j} \sim \text{E}(\lambda)$, where λ is the average arrival rate). In this paper, $\lambda = 1/180$, that is, the average arrival time interval of two adjacent vehicles is 3 min.

$$t_{\text{as}}^{i,k} = t_0 + \sum_{j=1}^{k} \tau_{\text{s}}^{i,j} \tag{1}$$

If there are no vehicles queuing ahead the kth EV when it arrives at the BSS, the waiting time of the kth EV is related to whether there is an idle swapping device or not. If there is no idle swapping device at that time, the kth EV needs to wait for the vehicle which finishes the service first. The waiting time can be calculated by the time when the vehicle finishes the service first minus the time when the kth EV arrives. If there is an idle swapping device, the waiting time is zero. Assuming $mt_{\text{ds}}^{i,k}$ to be the minimum value of the vehicles swapping-finish time at the swapping devices when the kth EV prepares for the next swapping (no vehicle queues ahead it), the determination of the waiting time for the kth EV $T_{\text{ws}}^{i,k}$ can be expressed by (2).

$$T_{\text{ws}}^{i,k} = \begin{cases} mt_{\text{ds}}^{i,k} - t_{\text{as}}^{i,k}, & \text{if } t_{\text{as}}^{i,k} < mt_{\text{ds}}^{i,k} \\ 0, & \text{if } t_{\text{as}}^{i,k} \geq mt_{\text{ds}}^{i,k} \end{cases} \tag{2}$$

After calculating the waiting time, the swapping-start time $t_{\text{ss}}^{i,k}$ and the swapping-finish time $t_{\text{os}}^{i,k}$ can be determined by (3) and (4), respectively, where $T_{\text{s}}^{i,k}$ is the swapping-duration time which follows a uniform distribution (in this paper, it is assumed that $T_{\text{s}}^{i,k} \sim U$ [5 min, 8 min]).

$$t_{\text{ss}}^{i,k} = t_{\text{as}}^{i,k} + T_{\text{ws}}^{i,k} \tag{3}$$

$$t_{\text{os}}^{i,k} = t_{\text{ss}}^{i,k} + T_{\text{s}}^{i,k} \tag{4}$$

If there are queues of vehicles ahead the kth EV when it arrives at the BSS, the waiting time of the kth EV can be determined by the recursive computation from the waiting time of the first in line. It is assumed that there are h vehicles queuing ahead the kth EV,

IET Gener. Transm. Distrib., 2016, Vol. 10, Iss. 4, pp. 1107–1116

then the waiting time, swapping-start time and swapping-finish time of the first in line (i.e. the $(k-h)$th vehicle) can be determined by (2)–(4) directly. When the $(k-h+1)$th vehicle prepares for the next swapping, it needs to update $mt_{ds}^{i,(k-h+1)}$ first. Then the waiting time, swapping-start time and swapping-finish time of the $(k-h+1)$th vehicle can be determined by (2)–(4). On the analogy of this, the waiting time of the kth EV can be determined finally.

$$mt_{ds}^{i,k} = \min\left(t_{ds,1}^{i,k}, t_{ds,2}^{i,k}, \ldots, t_{ds,d}^{i,k}\right) \tag{5}$$

The value of $mt_{ds}^{i,k}$ can be expressed as (5), where d is the number of swapping devices, $t_{ds,r}^{i,k}$ $(r=1, 2,\ldots,d)$ is the swapping-finish time of the vehicle at the rth swapping device when the kth EV prepares for the next swapping. The value of $t_{ds,r}^{i,k}$ $(r=1, 2,\ldots,d)$ is updating for each EV, which is determined as follows.

(i) if $k=1$, $t_{ds,r}^{i,k}=0$ $(r=1, 2,\ldots,d)$;
(ii) if $1<k\le d$, $t_{ds,r}^{i,k}=t_{os}^{i,r}$ $(r=1, 2,\ldots,k-1)$, $t_{ds,r}^{i,k}=0$ $(r=k, k+1, \ldots,d)$;
(iii) if $k=d+1$, $t_{ds,r}^{i,k}=t_{os}^{i,r}$ $(r=1, 2,\ldots,d)$;
(iv) if $k>d+1$, determine the value of $mt_{ds}^{i,(k-1)}$ and the corresponding swapping device number first (assumed to be q), then $t_{ds,r}^{i,k}=t_{ds,r}^{i,(k-1)}$ $(r=1, 2,\ldots,d, r\neq q)$, $t_{ds,r}^{i,k}=t_{os}^{i,(k-1)}$ $(r=q)$.

The stochastic analysis of the depleted batteries charging is similar to the analysis of vehicle batteries swapping described above. The main difference is that the arrival time of depleted batteries does not follow a Poisson process, but is determined by the swapping-finish time of EVs. It is assumed that the schedule charging power is P_{cs} (kW), charging efficiency is η_c, and the battery capacity is E_r (kWh), then the charging duration $T_c^{i,k}$ of the depleted battery from the kth EV is given by (6), where $SOC_0^{i,k}$ is the initial SOC of the depleted battery which follows a normal distribution (in this paper, it is assumed that $SOC_0^{i,k}\sim N(0.2, 0.1^2)$). After that, the waiting time for charging $T_{wc}^{i,k}$, the charging-start time $t_{sc}^{i,k}$ and the charging-finish time $t_{oc}^{i,k}$ can also be obtained like the computing method of those in the vehicle batteries swapping.

$$T_c^{i,k} = \frac{(0.85 - SOC_0^{i,k})E_r}{\eta_c P_{cs}} \tag{6}$$

The queues in vehicle batteries swapping and depleted batteries charging for the m EVs in each BSS can be simulated by the MCSS method such as the above analysis. Then the swapping-start time matrix $\boldsymbol{T}_{ss}$ $(=[t_{ss}^{i,k}]_{n\times m})$ of the $n\times m$ EVs and the charging-finish time matrix $\boldsymbol{T}_{oc}$ $(=[t_{oc}^{i,k}]_{n\times m})$ of the depleted batteries can be determined. By counting $\boldsymbol{T}_{ss}$ and $\boldsymbol{T}_{oc}$, we can obtain the vehicle swapping demand N_{sd} and the number of charged-up batteries N_{fc} at each time. Then the number of control-out batteries N_{out}, control-in batteries N_{in} and CBs N_c at time t can be calculated by (7)–(10), where N_0 is the number of batteries at the initial time (it is assumed that they are all in the controllable state) and η_r is batteries redundancy factor of the BSSs.

$$N_{out}(t) = \sum_{t_j=t_0}^{t} N_{sd}(t_j) \tag{7}$$

$$N_{in}(t) = \sum_{t_j=t_0}^{t} N_{fc}(t_j) \tag{8}$$

$$N_c(t) = N_0 - N_{out}(t) + N_{in}(t) \tag{9}$$

$$N_0 = mn(\eta_r - 1) \tag{10}$$

There are two kinds of CC, that is, controllable power capacity (CPC) and controllable energy capacity (CEC) which can be calculated by (11) and (12), respectively, where C_{s2g} (MW) is the CPC of BSS storage, E_c (MWh) is the CEC of BSS storage, and P_{bm} (kW) is the maximum charging/discharging power of the batteries.

$$C_{s2g}(t) = N_c(t)P_{bm}/1000 \tag{11}$$

$$E_c(t) = N_c(t)E_r/1000 \tag{12}$$

The flow chat of MCSS method for calculating the CC of BSSs is shown in Fig. 1. The computational procedure of this method is as follows.

(i) Initialise the parameters such as the number of BSSs and EVs, the average arrival time interval of EVs, the number of swapping devices and chargers, and so on.
(ii) Sample the arrival time intervals of EVs in the ith BSS according to the Poisson distribution and compute the arrival time of each vehicle by (1).

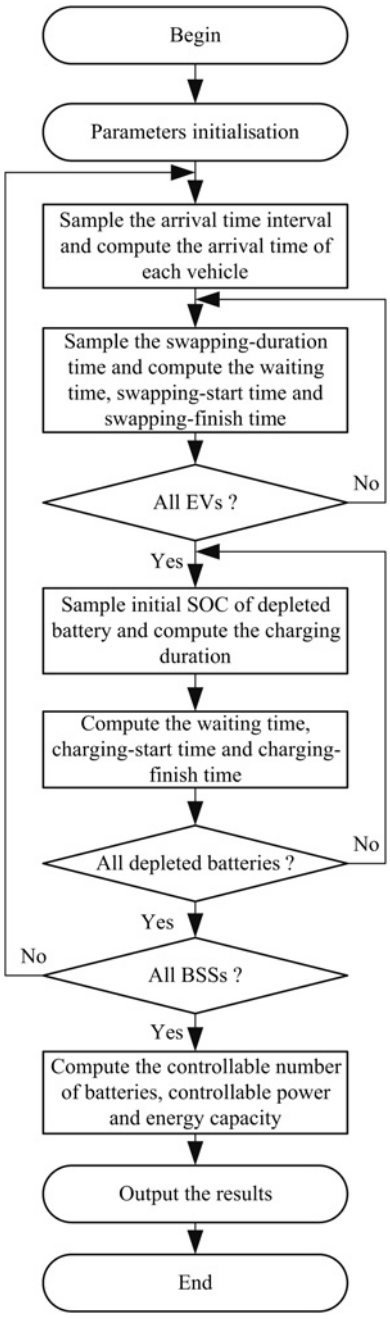

Fig. 1 *Flow chat of MCSS method for calculating the CC of BSSs*

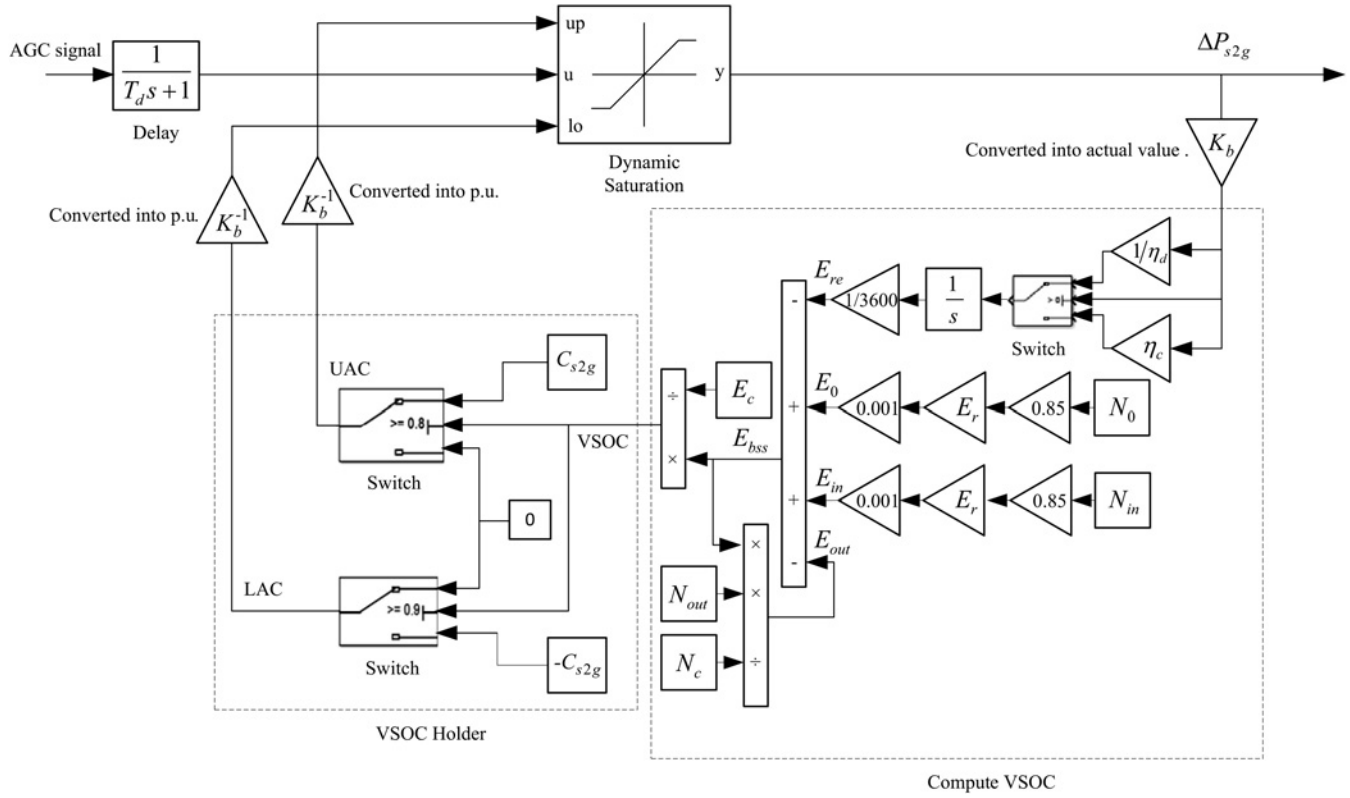

Fig. 2 *Lumped S2G equivalent model*

(iii) For the kth EV, sample the swapping-duration time according to the uniform distribution, update the values of $t_{\mathrm{ds},r}^{i,k}$ and $mt_{\mathrm{ds}}^{i,k}$, compute the waiting time, the swapping-start time and the swapping-finish time.

(iv) If it has traversed all the EVs, then sample the initial SOC of the depleted battery according to the normal distribution and compute the schedule charging duration by (6), else go to step (iii).

(v) Compute the waiting time for charging, the charging-start time and the charging-finish time of the depleted batteries.

(vi) If it has traversed all the depleted batteries, go to the next BSS, else go to step (iv).

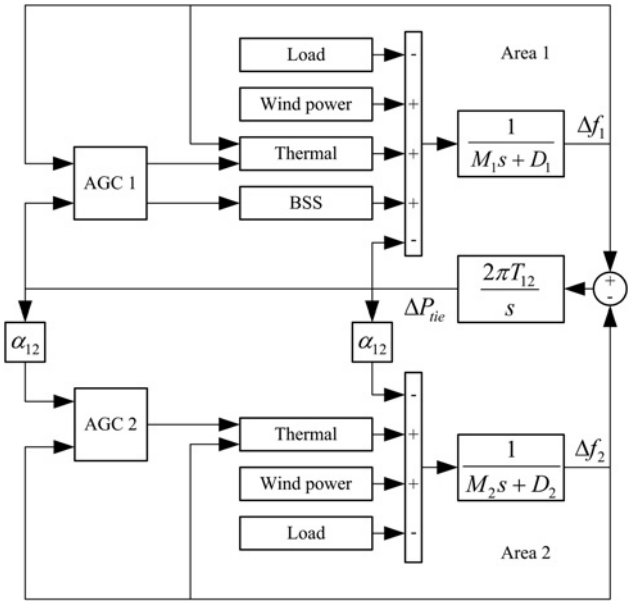

Fig. 3 *AGC model of a two-area interconnected power system considering S2G*

(vii) If it has traversed all the BSSs, then compute the number of CBs, CPC and CEC of BSSs, else go to step (ii).

(viii) Output the simulation results.

3.4 Lumped S2G model

The lumped S2G equivalent model for BSSs storage responding to the AGC signal as a VSS is designed as Fig. 2. The input of this model is the AGC signal for all the CBs in BSSs, and the output

Table 1 Data of power system

Parameter	Area 1	Area 2
maximum load capacity, MW	20,000	10,000
inertia constant, pu/Hz	0.64	0.32
load damping coefficient, pu/Hz	0.04	0.02
speed governor time constant, s	0.08	0.08
turbine time constant, s	0.3	0.3
droop control coefficient, Hz/pu	2.4	2.4
frequency bias factor, pu/Hz	0.15	0.075
dead band of primary frequency control, Hz	0.033	0.033
dead band of ACE, MW	20	10
ramp speed/(MW/min)	400	200
time constant for ACE calculation, s	2	2
communication delay, s	1	1
time constant of high–pass filter, s	60	60
time constant of low–pass filter, s	900	900
maximum load fluctuation, MW	457	255
maximum wind power fluctuation, MW	1316	440
tie-line synchronising coefficient, pu/Hz	0.0545	

Table 2 Technical parameters of BSS battery

Parameter	Value
battery capacity, kWh	60
maximum charging/discharging power, kW	15/15
schedule charging power, kW	9
charging/discharging efficiency	0.92/0.92
battery redundancy rate	1.3

IET Gener. Transm. Distrib., 2016, Vol. 10, Iss. 4, pp. 1107–1116

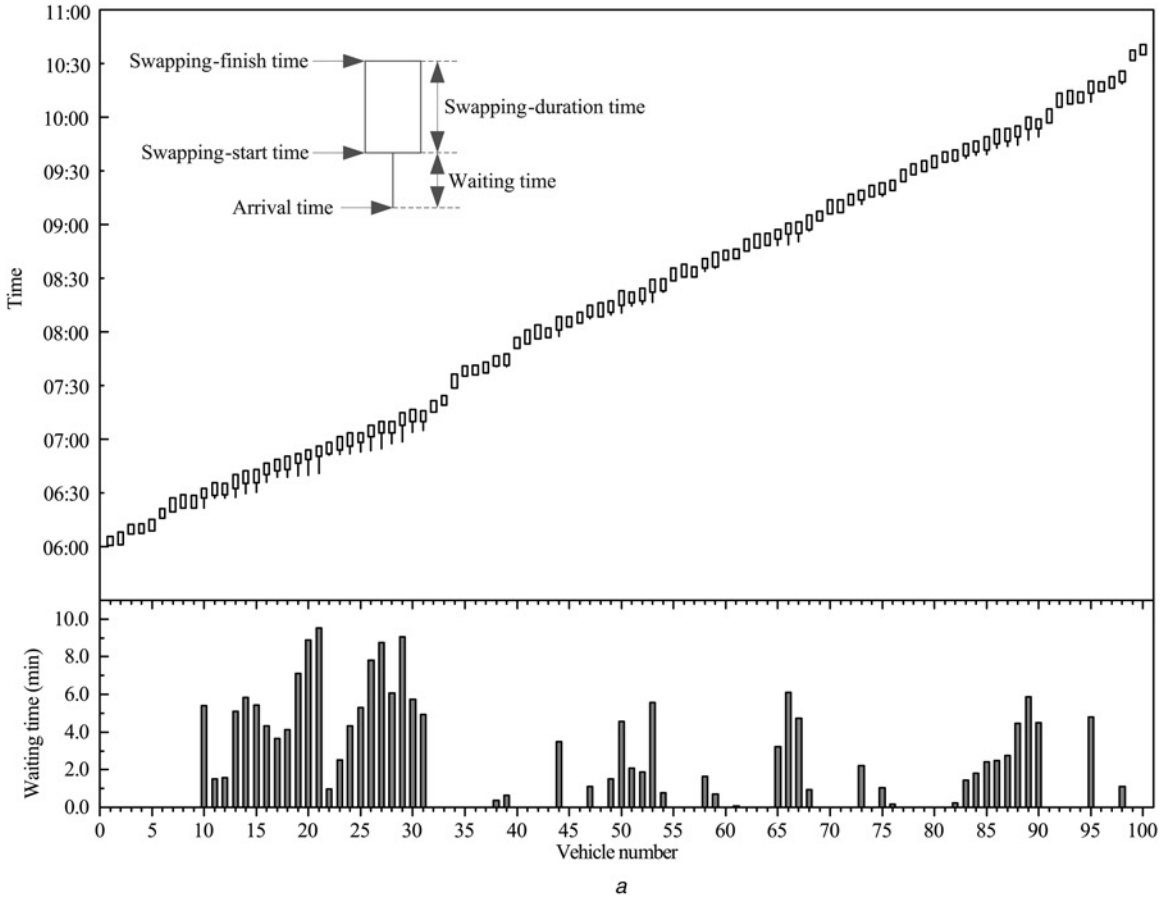

a

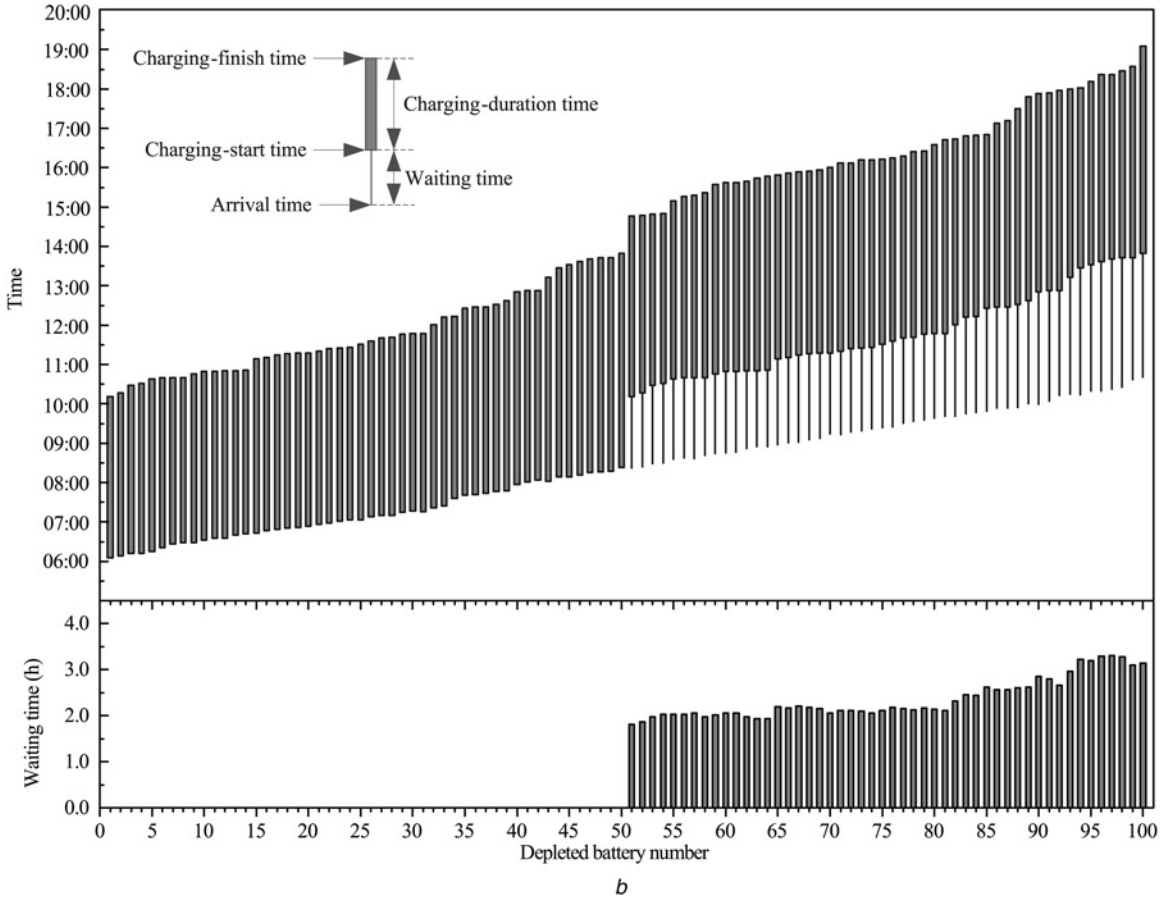

b

Fig. 4 *Queues in vehicle batteries swapping and depleted batteries charging*

a Time distribution of the first 100 vehicle batteries swapping in a BSS
b Time distribution of the first 100 depleted batteries charging in a BSS

Table 3 Numerical characteristics of the queues in the first 100 vehicle batteries swapping and depleted batteries charging

	Vehicle batteries swapping			Depleted batteries charging		
	Arrival time interval/min	Waiting time/min	Swapping-duration time/min	Arrival time interval/min	Waiting time/h	Charging-duration time/h
max	13.29	9.51	8.00	12.13	3.31	5.43
min	0.09	0	5.05	0.10	0	4.08
ave	2.75	1.93	6.43	2.96	1.18	4.67
SD	2.73	2.59	0.87	2.33	1.22	0.31

is the total charging/discharging responsive power of the CBs. The communication delay is approximated by a first-order model with time delay denoted by T_d. A dynamic VSOC holder is developed to keep VSOC between 0.8 and 0.9 by adjusting the upper and lower limit of the saturation element in real time subject to the constraints of VSOC and CC. The upper and lower limits are determined by (13) and (14), respectively, where UAC is the upper limit of the available capacity, and LAC is the lower limit of the available capacity. It can be seen from the strategy that only when VSOC is between 0.8 and 0.9, the BSSs can respond to the AGC signal freely. If VSOC is lower than 0.8, UAC will be set to zero, which means only charging signal can be responded (the discharging power is defined as positive in this paper). If VSOC is higher than 0.9, LAC will be set to zero, which means only discharging signal can be responded.

$$\mathrm{UAC} = \begin{cases} C_{\mathrm{s2g}}, & \mathrm{VSOC} \geq 0.8 \\ 0, & \mathrm{VSOC} < 0.8 \end{cases} \tag{13}$$

$$\mathrm{LAC} = \begin{cases} 0, & \mathrm{VSOC} \geq 0.9 \\ -C_{\mathrm{s2g}}, & \mathrm{VSOC} < 0.9 \end{cases} \tag{14}$$

The VSOC can be expressed as (15), where $E_{\mathrm{bss}}(t)$ is the total stored energy of CBs at time t. The real time value of $E_{\mathrm{bss}}(t)$ during regulation can be calculated by (16), which consists of the initial stored energy E_0, the total increased energy $E_{\mathrm{in}}(t)$ due to the control-in of the batteries, the total decreased energy $E_{\mathrm{out}}(t)$ due to the control-out of the batteries, and the energy change $E_{\mathrm{re}}(t)$ due to the participation of BSSs in AGC program.

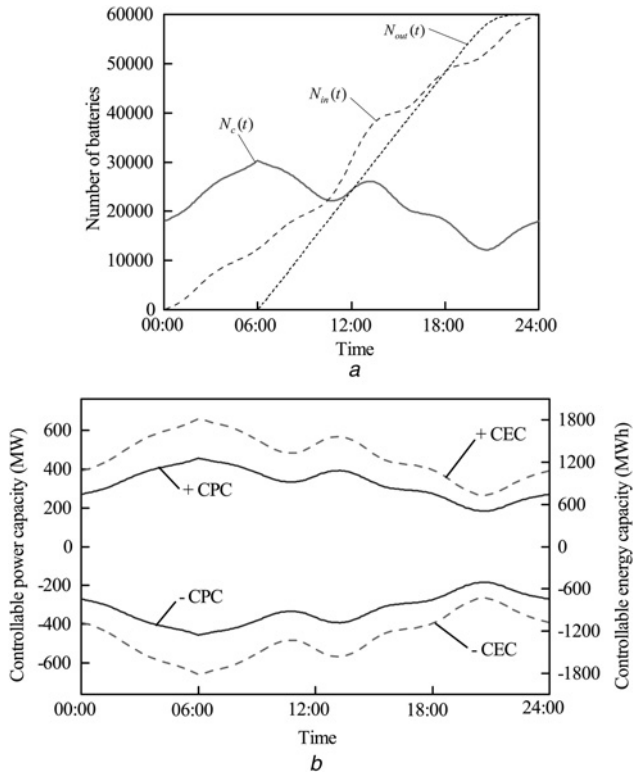

Fig. 5 *Number of CBs and the CC of BSS storage*

a Number of CBs, control-in, and control-out batteries
b CPC and CEC of BSS storage

$$\mathrm{VSOC}(t) = E_{\mathrm{bss}}(t)/E_{\mathrm{c}}(t) \tag{15}$$

$$E_{\mathrm{bss}}(t) = E_0 + E_{\mathrm{in}}(t) - E_{\mathrm{out}}(t) - E_{\mathrm{re}}(t) \tag{16}$$

The values of E_0, $E_{\mathrm{in}}(t)$, and $E_{\mathrm{out}}(t)$ are related to the number of batteries in its state and can be determined by (17)–(19), respectively, while $E_{\mathrm{re}}(t)$ is related to the power conversions between the grid and batteries. Power loss such as the charging/discharging loss and leakage loss may exist in the inverters and transformers. In this paper, we select the charging efficiency η_{c} and discharging efficiency η_{d} to reflect the overall power loss between the grid and batteries. Thus, the calculation of $E_{\mathrm{re}}(t)$ can be expressed by (20), where $\Delta P_{\mathrm{s2g}}(t')$ is the responsive power of BSSs at the grid side, $\boldsymbol{I}(\cdot)$ is the indicator function, and K_{b} is the base power for conversions between the p.u. and actual value. $\Delta P_{\mathrm{s2g}}(t') > 0$ means that the BSSs need to offer regulation up service by discharging the batteries (at this time, $\boldsymbol{I}(\Delta P_{\mathrm{s2g}}(t') > 0) = 1$, $\boldsymbol{I}(\Delta P_{\mathrm{s2g}}(t') < 0) = 0$), while $\Delta P_{\mathrm{s2g}}(t') < 0$ means that the BSSs need to offer regulation down service by charging the batteries (at this time, $\boldsymbol{I}(\Delta P_{\mathrm{s2g}}(t') > 0) = 0$, $\boldsymbol{I}(\Delta P_{\mathrm{s2g}}(t') < 0) = 1$). The VSOC holder and the indicator function can be achieved by switch blocks in Matlab/Simulink.

$$E_0 = 0.85 N_0(t) E_{\mathrm{r}}/1000 \tag{17}$$

$$E_{\mathrm{in}}(t) = 0.85 N_{\mathrm{in}}(t) E_{\mathrm{r}}/1000 \tag{18}$$

$$E_{\mathrm{out}}(t) = N_{\mathrm{out}}(t) E_{\mathrm{bss}}(t)/N_{\mathrm{c}}(t) \tag{19}$$

$$\begin{aligned} E_{\mathrm{re}}(t) = \int_0^t \Big(& \frac{1}{\eta_{\mathrm{d}}} K_{\mathrm{b}} \Delta P_{\mathrm{s2g}}(t') \boldsymbol{I}(\Delta P_{\mathrm{s2g}}(t') > 0) \\ & + \eta_{\mathrm{c}} K_{\mathrm{b}} \Delta P_{\mathrm{s2g}}(t') \boldsymbol{I}(\Delta P_{\mathrm{s2g}}(t') < 0) \Big) \, \mathrm{d}t'/3600 \end{aligned} \tag{20}$$

4 AGC model considering S2G

4.1 Simulation model of power system with BSSs

A two-area interconnected power system model is considered, in which all generators participating in frequency regulation are lumped as a single equivalent generating unit. The simulation model is illustrated in Fig. 3, where M_i, D_i is the inertia constant and the load damping coefficient of area i ($i = 1, 2$), respectively, $\Delta f_i$is the frequency deviation of area i ($i = 1, 2$), ΔP_{tie} is the tie-line power deviations, α_{12} is the negative ratio between rated capacity of area 1 and 2, T_{12} is the synchronising coefficient. The 'thermal' block which represents the model of thermal units with the constraints of governor dead-band, generation rate constraint and communication delay can be found in [29], and the 'BSS' block is shown in Fig. 2. Random load and wind power in a time series are used for frequency regulation simulation [30], which consist of a slow base component with large amplitude and a fast fringe component with small amplitude. Tie-line bias control [31] is used for the interconnected power system.

IET Gener. Transm. Distrib., 2016, Vol. 10, Iss. 4, pp. 1107–1116

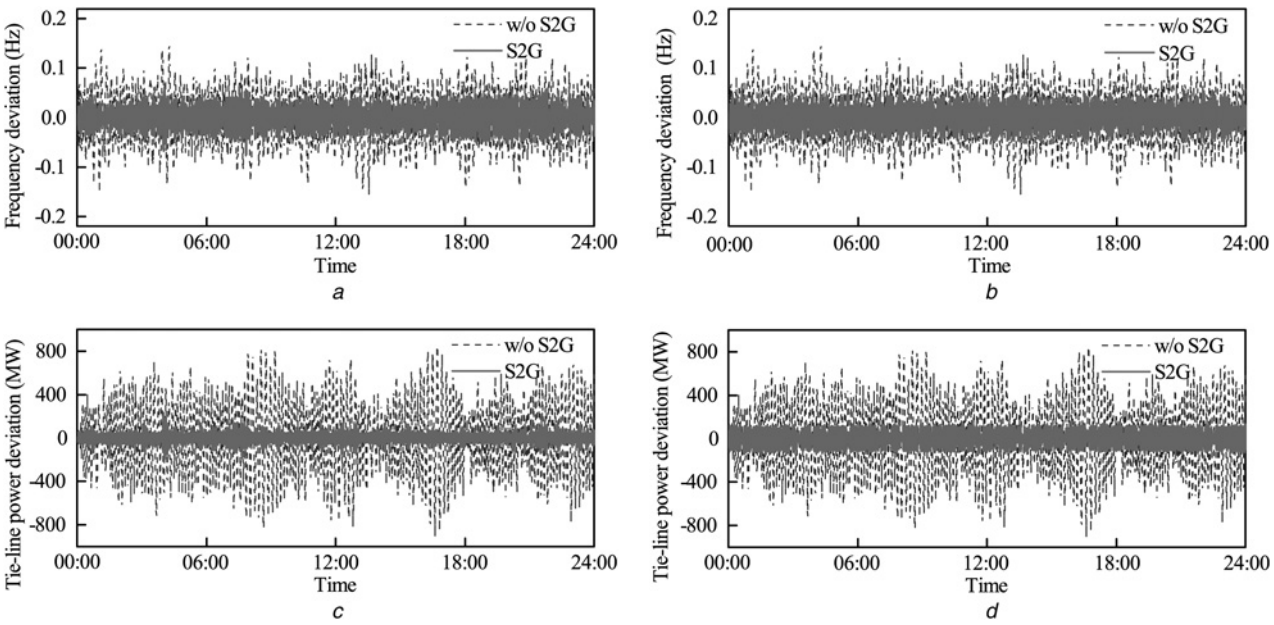

Fig. 6 *Frequency and tie-line power deviations*

a Frequency deviation in Case 1
b Frequency deviation in Case 2
c Tie-line power deviation in Case 1
d Tie-line power deviation in Case 2

4.2 Filter-based coordinated control strategy

In this paper, we propose a filter-based coordinated control strategy to distribute the control signal between the slower thermal units and the fast BSSs storage. By filtering the output of the PI controller, the control signal can be divided into three parts, that is, fast-cyclic component (less than 1 min), short-cyclic component (1–15 min), and long-cyclic component (more than 15 min). The long-cyclic component is mainly regulated by the economic dispatch program and should not be considered here. The BSSs storage can follow the fast-cyclic component, whereas the thermal units can follow the short-cyclic component. In this way, the required capacity of BSSs storage can be reduced, and the thermal units can be operated at steadier conditions.

5 Simulation results

5.1 Initial conditions

The effectiveness of the proposed model and control strategies under a significant random load and wind power fluctuations is studied based on a two-area interconnected system. The data of the system is shown in Table 1. The number of BSSs in the control area is assumed to be 200. In each BSS, there are three swapping devices and 50 chargers, which means it can provide services for three EVs and 50 depleted batteries furthest at the same time. The number of EVs arriving at each BSS for batteries swapping is assumed to be 300 equally, that is to say, the total number of EVs for batteries swapping is 60,000. The initial time of battery swapping is assumed to be 06:00 am. The probability distributions of the arrival time interval, the swapping-duration time, and the initial SOC of the depleted batteries have been given in Section 3.3. The parameters of batteries are given in Table 2.

5.2 Analysis of the queues in vehicle batteries swapping and depleted batteries charging

To show the queues in batteries swapping and charging intuitively, we take the first 100 EVs as well as their depleted batteries in a randomly selected BSS as an example. The results are shown in Fig. 4 in the form of candlestick charts. It can be seen that the waiting time of one vehicle is depended on the minimum swapping-finish time of the three vehicles ahead of it. If the candlestick bottom of this vehicle is higher than the lowest box top of the three vehicles ahead of it, the waiting time is zero. Otherwise, the waiting time is the height difference between the two. For the vehicle which needs to wait for the service, the box bottom is at the same height with the lowest box top of the three vehicles ahead of it, which means that the vehicle will accept the service immediately as long as one of the three vehicles has finished. The similar conclusions can be obtained for the depleted batteries charging. Because the time interval between one depleted battery and the 50th battery ahead of it is shorter than charging-duration time of the 50th battery ahead, the depleted batteries after the first 50 batteries may need to wait for charging.

The maximum (Max), minimum (Min), average (Ave) and standard deviation (SD) values of the arrival time interval, waiting time and duration time of the queues in the first 100 vehicle batteries swapping and their depleted batteries charging are shown in Table 3. It can be seen that the maximum waiting time of the vehicle batteries swapping is approximately equal to the average arrival time interval multiplies the number of swapping devices. The average arrival time interval of depleted batteries is approximately equal to that of vehicles because of their one-to-one relationship.

5.3 Number of CBs and the CC of BSS storage

The changes of number of CBs, control-in, and control-out batteries are shown in 3.5*a*. The maximum number of CBs is 3,0216 which happens at 06:00 am. With the control-in and control-out of batteries due to the depleted batteries charging and vehicle batteries swapping, the number of CBs changes dynamically. The minimum number of CBs is 1,2187. The changes of CPC and CEC of BSS storage are shown in Fig. 5*b*. The maximum value of CPC and CEC are 454.74 MW and 1819 MWh, while the minimum value are 182.81 MW and 731.22 MWh, respectively.

5.4 Impacts of S2G on AGC performance

Three simulation cases are performed and compared to validate the effects of S2G regulation on the dynamic performance of AGC.

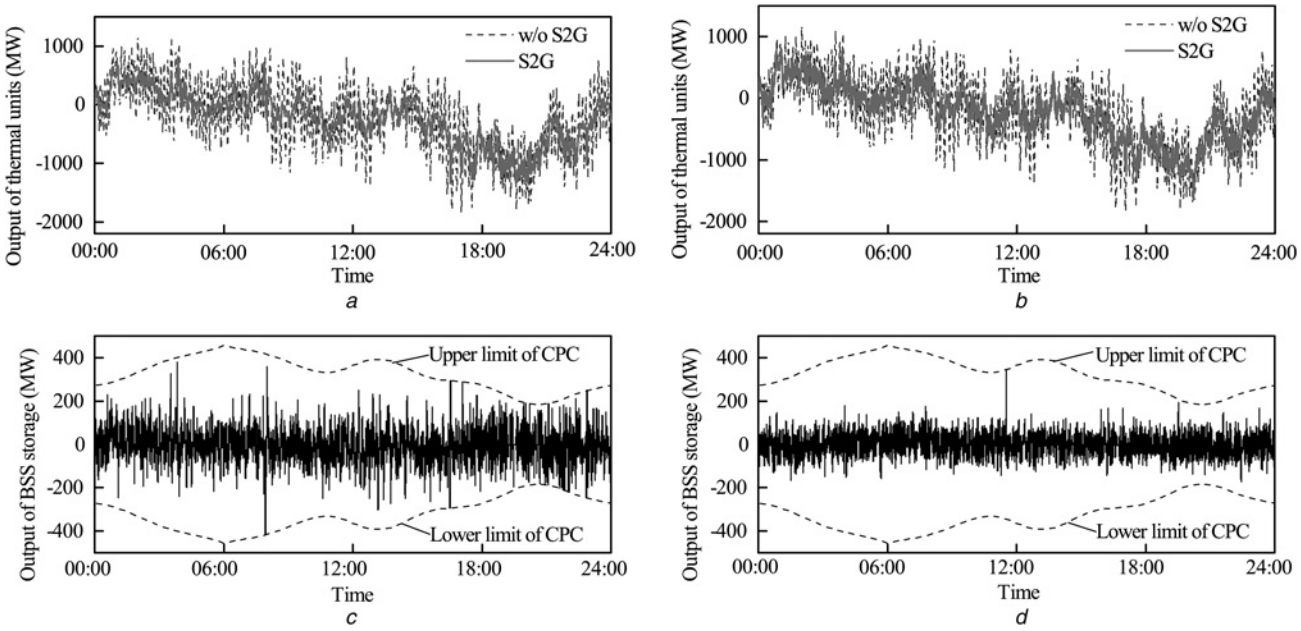

Fig. 7 *Outputs of thermal units and BSS storage*

a Output of thermal units in Case 1
b Output of thermal units in Case 2
c Output of BSS storage in Case 1
d Output of BSS storage in Case 2

The simulation without BSS storage (Case 0), where only the thermal units participate in AGC is considered as the first or reference case. The remaining cases are the simulation with BSS storage located in area 1 (Case 1) and the simulation with BSS storage located in area 2 (Case 2). The difference between Case 1 and Case 2 is that the unbalance power of the area where the BSS storage is located is different. In fact, the unbalance power of area 1 is larger than that of area 2. The frequency deviation of area 1, the tie-line power deviation, the output of thermal units in area 1, and the output of BSS storage are selected to show the effects of S2G regulation on them.

Compared to Case 0, the fluctuations of frequency and tie-line power deviations are suppressed significantly in Case 1 and Case 2, as shown in Fig. 6. The tie-line power deviation in Case 1 is even smaller than that in Case 2. This is because the larger unbalance power of area 1 has been regulated by the BSS storage.

Table 4 Comparisons of system responses in different scenarios

		Case 0	Case 1	Case 2
frequency deviation in area 1	Max/Hz	0.1460	0.0578	0.0651
	Min/Hz	−0.1551	−0.0670	−0.0682
	RMS/Hz	0.0605	0.0113	0.0184
tie-line power deviation	Max/MW	840.52	131.31	164.94
	Min/MW	−903.74	−116.18	−183.35
	RMS/MW	324.50	44.08	51.09
output of thermal units in area 1	Max/MW	1164.62	719.79	816.30
	Min/MW	−1830.64	−1466.87	−1639.02
	RMS/MW	605.44	486.97	501.87
output of thermal units in area 2	Max/MW	1090.93	663.27	528.35
	Min/MW	−968.94	−494.08	−453.48
	RMS/MW	367.82	192.73	176.31
output of BSS storage	Max/MW	–	380.37	343.85
	Min/MW	–	−416.69	−173.75
	RMS/MW	–	74.05	45.14

Fig. 7 shows the outputs of thermal unit and BSS storage. The output of thermal unit in Case 1 and Case 2 are reduced greatly

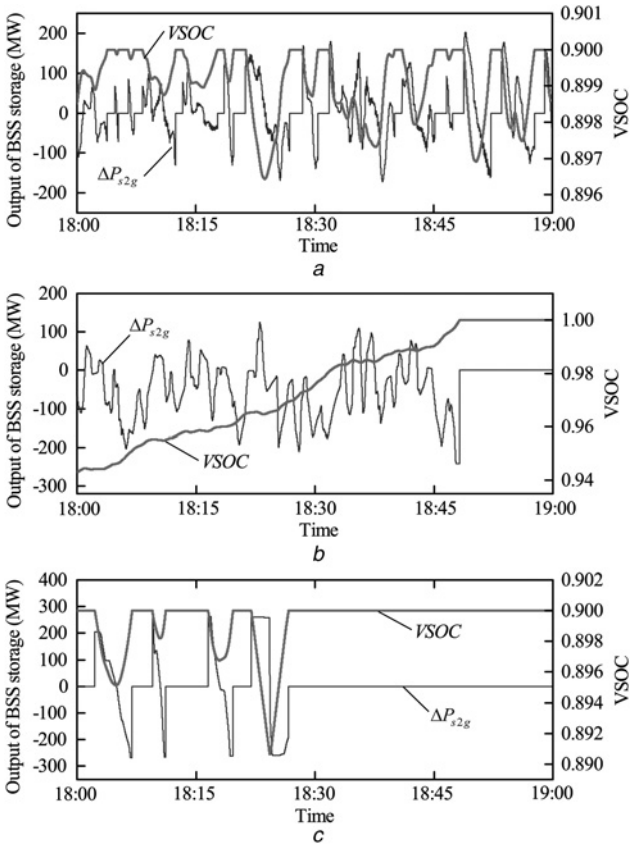

Fig. 8 *Output of BSS storage and VSOC from 18:00 to 19:00*

a Output of BSS storage and VSOC in Case 1
b Output of BSS storage and VSOC in Case 3
c Output of BSS storage and VSOC in Case 4

IET Gener. Transm. Distrib., 2016, Vol. 10, Iss. 4, pp. 1107–1116

Table 5 Hourly revenue, cost and income of S2G regulation

Hour	EMCP, $/MWh	RMCP, $/MWh	Case 1			Case 2		
			Revenue, $	Cost, $	Income, $	Revenue, $	Cost, $	Income, $
1	51.09	39.63	2322.28	6007.95	−3685.67	2323.55	2634.15	−310.60
2	49.08	62.63	3812.98	8237.62	−4424.64	3928.43	5374.80	−1446.37
3	37.68	44.48	3633.85	5116.11	−1482.26	3317.66	2885.03	432.63
4	35.98	30.61	2529.28	1283.17	1246.11	2391.33	1390.23	1001.1
5	35.92	31.84	2687.42	1032.06	1655.36	2680.42	3979.55	−1299.13
6	43.98	51.76	4564.50	1613.18	2951.32	4517.28	2076.45	2440.83
7	33.65	85.60	8633.67	2329.01	6304.66	8288.85	5444.92	2843.93
8	44.42	44.09	3989.78	3043.15	946.63	4136.97	5913.40	−1776.43
9	45.40	38.33	3235.57	2229.44	1006.13	3075.88	1742.23	1333.65
10	92.21	112.00	8476.15	995.43	7480.72	8051.98	358.13	7693.85
11	84.74	149.24	11466.24	8723.11	2743.13	10728.62	1407.63	9320.99
12	119.30	260.87	19938.64	4122.73	15815.91	19252.02	480.09	18771.93
13	61.65	66.73	5325.33	5578.82	−253.49	5265.05	1115.46	4149.59
14	38.77	46.41	3567.04	2734.41	832.63	3540.15	2718.56	821.59
15	39.06	37.37	2546.05	1445.01	1101.04	2596.21	1575.53	1020.68
16	52.55	94.97	5824.98	7593.64	−1768.66	6073.05	1464.45	4608.6
17	136.90	332.56	20154.17	8369.21	11784.96	19686.97	464.29	19222.68
18	64.84	90.10	5737.66	1798.32	3939.34	5886.80	733.12	5153.68
19	78.66	84.94	4401.53	2663.20	1738.33	4565.43	2325.22	2240.21
20	55.21	66.67	3517.90	2310.81	1207.09	2990.41	4176.79	−1186.38
21	42.48	28.95	1164.81	1217.93	−53.12	1208.07	1410.03	−201.96
22	36.26	47.07	2386.72	952.84	1433.88	1909.91	1897.62	12.29
23	34.01	46.96	2638.31	2227.41	410.90	2372.74	4203.60	−1830.86
24	27.31	21.75	1409.23	1393.82	15.41	1277.22	619.33	657.89
total	–	–	133964.10	83018.38	50945.72	130065	56390.61	73674.39

due to the participation of S2G. The output of BSS storage in Case 1 is larger than that in Case 2 because of the larger unbalance power of area 1. Wherever the BSS storage, the S2G power is kept within the allowable range of CPC.

In addition, max values, min values, and root mean square (RMS) values of the system responses including frequency deviation in area 1, tie-line power deviation, output of thermal unit in area 1 and 2, and output of BSS storage are summarised in Table 4. It can be seen that the control performance of AGC system is totally improved by the S2G regulation.

5.5 Effectiveness of proposed control strategies

We select the output of BSS storage and its VSOC during the time slot between 18:00 and 19:00 to analyse the impacts of different control strategies on them, that is, the control strategy without VSOC holder (Case 3) and that without the filter-based coordinated strategy (Case 4), compared to the scenario using both of the VSOC holder and filter-based coordinated control strategies in Case 1. The BSS storage is located in area 1 where an excess generation needs to be absorbed during this time slot. The maximum excess generation is 1105 MW at the time near 18:30. The maximum CPC of BSS storage during this time slot is 273 MW. The strong charging demand will lead to a quick increment in VSOC and make the BSS storage operate near the SOC limits. The impacts of different control strategies on the output of BSS storage and its VSOC during the time slot are shown in Fig. 8.

In Fig. 8*a*, the VSOC of BSS storage is limited between 0.8 and 0.9 strictly by VSOC holder in Case 1, although there is a strong demand of charging batteries during this time slot. The charging power becomes 0 when VSOC is equal to 0.9, which means that the BSS storage will not respond to the control signal. However, due to the filter-based coordinated control strategy, the BSS storage can still respond to a fast-cyclic component of the discharging control signal. The fast-cyclic discharging can reduce VSOC below 0.9 temporarily so that the BSS storage can continue to absorb the excess power.

Without VSOC holder, the VSOC is lifted up to 1 because of the strong charging demand, as shown in Fig. 8*b*. When VSOC is equal to 1, which means all of the CBs has been fully charged, the control signal will not be responded any more. While without of a filter-based coordinated control, a larger portion of the control signal is dispatched to the BSS storage, which makes the BSS storage operate at the maximum CPC and quickly drop out of AGC, as shown in Fig. 8*c*. The control signal will not be responded any more at the time near 18:30 when the maximum excess generation happens.

5.6 Economic analysis of S2G regulation

The economic feasibility of S2G regulation is analysed using the cost-benefit analysis method [12] based on the PJM energy and regulation market pricing. The revenue is derived from two parts: (i) a capability payment for the capacity held in reserve, and (ii) a mileage performance payment based on the amount of up and down movement in response to a control signal [32]. The cost to produce regulation is calculated as the cost to purchase the dispatched energy plus the battery degradation cost, and the fixed cost for additional equipment needed for S2G [12]. The data of PJM hourly energy market clearing price (EMCP) and regulation market clearing price (RMCP) dated on 01-March-2015 [33] are used to calculate the revenues, costs and incomes of Case 1 and Case 2. The results are shown in Table 5. The daily incomes of Case 1 and Case 2 are $50945.72 and $73674.39, respectively. This hence can encourage the inclusion of BSS energy storage into the frequency regulation service.

6 Conclusions

With the standardisation of electric vehicle battery technologies and the continuous construction of BSSs, the energy supply based on battery swapping will be widely applied. From the point view of the power grid, BSS is a good controllable energy resource, which is able to participate in AGC program. Furthermore, the application of energy storage in BSSs will significantly change the conventional power system frequency control framework. The regulation resources in both the generation side and demand side are used to maintain the frequency stability of power systems.

This paper analyses the capability of providing supplementary frequency control using the controllable energy storage in BSSs. The MCSS method is utilised to estimate the CC of BSS storage by emulating the queues in batteries swapping and charging. A lumped equivalent S2G model considering the battery SOC limits and CC constrains is proposed. The filter-based coordinated control strategy is used in the AGC model considering S2G. The

proposed AGC strategies are verified in a two-area interconnected power system with relatively large random load and wind power fluctuations. The simulation results and economic analysis demonstrates the availability of the proposed models and control methods.

7 Acknowledgments

This work was supported by the National High Technology Research and Development of China (863 Program) (2011AA05A109).

8 References

1 Doherty, R., Mullane, A., Nolan, G., *et al.*: 'An assessment of the impact of wind generation on system frequency control', *IEEE Trans. Power Syst.*, 2010, **25**, (1), pp. 452–460
2 Zhu, D., Hug-Glanzmann, G.: 'Coordination of storage and generation in power system frequency control using an H-infinity approach', *IET Gener. Transm. Distrib.*, 2013, **7**, (11), pp. 1263–1271
3 Xue, Y., Tai, N.: 'Review of contribution to frequency control through variable speed wind turbine', *Renew. Energy*, 2011, **36**, (6), pp. 1671–1677
4 Hanley, M., Ilic, J.: 'Frequency instability problems in north American interconnections' (National Energy Technology Laboratory, USA, 2011)
5 Zhao, X., Ostergaard, J., Togeby, M.: 'Demand as frequency controlled reserve', *IEEE Trans. Power Syst.*, 2011, **26**, (3), pp. 1062–1071
6 Masoum, A.S., Deilami, S., Moses, P.S., *et al.*: 'Smart load management of plug-in electric vehicles in distribution and residential networks with charging stations for peak shaving and loss minimization considering voltage regulation', *IET Gener. Transm. Distrib.*, 2011, **5**, (8), pp. 877–888
7 Huang, H., Chung, C., Chan, K., *et al.*: 'Quasi-monte carlo based probabilistic small signal stability analysis for power systems with plug-in electric vehicle and wind power integration', *IEEE Trans. Power Syst.*, 2013, **28**, (3), pp. 3335–3343
8 Gholami, A., Ansari, J., Jamei, M., *et al.*: 'Environmental/economic dispatch incorporating renewable energy sources and plug-in vehicles', *IET Gener. Transm. Distrib.*, 2014, **8**, (12), pp. 2183–2198
9 Esmaili, M., Rajabi, M.: 'Optimal charging of plug-in electric vehicles observing power grid constraints', *IET Gener. Transm. Distrib.*, 2014, **8**, (4), pp. 583–590
10 Ortega-Vazquez, M.A.: 'Optimal scheduling of electric vehicle charging and vehicle-to-grid services at household level including battery degradation and price uncertainty', *IET Gener. Transm. Distrib.*, 2014, **8**, (6), pp. 1007–1016
11 Kempton, W., Tomic, J.: 'Vehicle-to-grid power fundamentals: calculating capacity and net revenue', *J. Power Sources*, 2005, **144**, (1), pp. 268–279
12 Tomic, J., Kempton, W.: 'Using fleets of electric-drive vehicles for grid support', *J. Power Sources*, 2007, **168**, (2), pp. 459–468
13 Ota, Y., Taniguchi, H., Nakajima, T., *et al.*: 'Autonomous distributed V2G (vehicle-to-grid) satisfying scheduled charging', *IEEE Trans. Smart Grid*, 2012, **3**, (1), pp. 559–564
14 Liu, H., Hu, Z., Song, Y., *et al.*: 'Decentralized vehicle-to-grid control for primary frequency regulation considering charging demands', *IEEE Trans. Power Syst.*, 2013, **28**, (3), pp. 3480–3489
15 Yang, H., Chung, C., Zhao, J.: 'Application of plug-in electric vehicles to frequency regulation based on distributed signal acquisition via limited communication', *IEEE Trans. Power Syst.*, 2013, **28**, (2), pp. 1017–1026
16 Pillai, J.R., Jensen, B.B.: 'Integration of vehicle-to-grid in the Western Danish power system', *IEEE Trans. Sust. Energy*, 2011, **2**, (1), pp. 12–19
17 Masuta, T., Yokoyama, A.: 'Supplementary load frequency control by use of a number of both electric vehicles and heat pump water heaters', *IEEE Trans. Smart Grid*, 2012, **3**, (3), pp. 1253–1262
18 Zheng, Y., Dong, Z., Xu, Y., *et al.*: 'Electric vehicle battery charging/swap stations in distribution systems: comparison study and optimal planning', *IEEE Trans. Power Syst.*, 2014, **29**, (1), pp. 221–229
19 Dai, Q., Cai, T., Duan, S., *et al.*: 'Stochastic modeling and forecasting of load demand for electric bus battery-swap station', *IEEE Trans. Power Deliv.*, 2014, **29**, (4), pp. 1909–1917
20 Armstrong, M., Moussa, C.E.H., Adnot, J., *et al.*: 'Optimal recharging strategy for battery-switch stations for electric vehicles in France', *Energy Policy*, 2013, **60**, pp. 569–582
21 Sarker, M.R., Pandzic, H., Ortega-Vazquez, M.A.: 'Optimal operation and services scheduling for an electric vehicle battery swapping station', *IEEE Trans. Power Syst.*, 2015, **30**, (2), pp. 901–910
22 Rao, R., Zhang, X., Xie, J., *et al.*: 'Optimizing electric vehicle users' charging behavior in battery swapping mode', *Appl. Energy*, 2015, **155**, pp. 547–559
23 Yang, S., Yao, J., Kang, T., *et al.*: 'Dynamic operation model of the battery swapping station for EV (electric vehicle) in electricity market', *Energy*, 2014, **65**, pp. 544–549
24 Takagi, M., Iwafune, Y., Yamaji, K., *et al.*: 'Economic value of PV energy storage using batteries of battery-switch stations', *IEEE Trans. Sust. Energy*, 2013, **4**, (1), pp. 164–173
25 Liu, N., Chen, Z., Liu, J., *et al.*: 'Multi-objective optimization for component capacity of the photovoltaic-based battery switch stations: towards benefits of economy and environment', *Energy*, 2014, **64**, pp. 779–792
26 Liu, N., Chen, Q., Lu, X., *et al.*: 'A charging strategy for PV-based battery switch stations considering service availability and self-consumption of PV Energy', *IEEE Trans. Ind. Electron.*, 2015, **62**, (8), pp. 4878–4889
27 Shimizu, K., Masuta, T., Ota, Y., *et al.*: 'A new load frequency control method in power system using vehicle-to-grid system considering users' convenience'. 17th Power Systems Computation Conf., Zurich, Switzerland, IEEE, 2011, pp. 1–7
28 Bhat, U.N.: 'An introduction to queueing theory: modeling and analysis in applications' (Birkhäuser Boston & Springer Science, New York, 2008), pp. 43–50
29 Lu, C., Liu, C., Wu, C.: 'Effect of battery energy storage system on load frequency control considering governor deadband and generation rate constraint', *IEEE Trans. Energy Convers.*, 1995, **10**, (3), pp. 555–561
30 Michigami, T., Ishii, T.: 'Construction of fluctuation load model and dynamic simulation with LFC control of DC power system and frequency converter interconnection'. Proc. IEEE Power Engineering Society Transmission and Distribution Conf., Yokahama, Japan, October 2002, pp. 382–387
31 Kunder, P.: 'Power system stability and control' (McGraw-Hill, New York, USA, 1994), pp. 606–610
32 Krishnan, V., Das, T., McCalley, J.D.: 'Impact of short-term storage on frequency response under increasing wind penetration', *J Power Sources*, 2014, **257**, (2), pp. 111–119
33 'PJM regulation zone preliminary billing data', http://www.pjm.com/markets-and-operations/billing-settlements-and-credit/preliminary-billing-reports/pjm-reg-data.aspx